**Supporting Information**

# Zero-Wastewater Capacitive Deionization: Selective Removal of Heavy Metal Ions in Tap Water Assisted by Phosphate Ions

Xingkang Huang,[a,†,*] Xiaoru Guo,[a,†] Qianqian Dong,[a] Lianjun Liu,[b] Rebecca Tallon,[b] and Junhong Chen[a*]

[a]Department of Mechanical Engineering, University of Wisconsin-Milwaukee, 3200 North Cramer Street, Milwaukee, WI, 53211, USA.

[b] A.O. Smith Corporation, Corporate Technology Center, 12100 W Park Place， Milwaukee, WI, 53224, USA.

## Experimental

Lead(II) nitrate, calcium chloride dehydrates, and magnesium chloride hexahydrate were used as purchased. Nitric acid (67%) was used as a digester for the ion concentration tests. Polyvinylidene fluoride (PVDF) and N-methyl-2-pyrrolidone (NMP) were purchased from Sigma-Aldrich and used to prepare the coating slurries. Ultrapure water (Millipore, U.S.A.) was used to prepare the feeding solution. Activated carbon (YP50F, Sanwa) was used as the baseline material, with a surface area of ~1694 $m^2\ g^{-1}$ as measured by $N_2$ adsorption/desorption on a Micromeritics ASAP 2020. X-ray photoelectron spectroscopy (XPS) spectra of samples were obtained using a PerkinElmer PHI 5440 ESCA spectrometer with monochromatic Mg Kα radiation as the X-ray source. Anion-exchange membrane (AEM, FAS-PET-130) was purchased from FUMATECH BWT GmbH.

First, 2 g of graphene oxide (GO) was dispersed in 50 mL concentrated nitric acid and heated for 2 h while stirring. The acid-treated GO was washed twice with DI water and three times with absolute ethanol, and then dispersed in 200 mL absolute ethanol with the help of sonication, resulting in GO dispersion (10 mg/mL). Then, 6 mg of 3-(Mercaptopropyl)trimethoxysilane (MPS) was added to 30 mL GO dispersion and heated at 60 for 4h. The MPS-modified GO (MPS-GO) was washed three times with absolute ethanol, and then mixed with 0.7 g of activated carbon in 50 mL ethanol. The mixture was stirred in a fume hood to obtain a dried MPS-GO/AC composite, which was dried overnight under vacuum at 60 °C and then ground to pass through a 325-mesh sieve.

The morphologies of the as-prepared sample were characterized by scanning electron microscopy (SEM) and energy-dispersive X-ray spectroscopy (EDS), performed on a Hitachi S-4800 SEM machine equipped with a Bruker EDS detector. Powder X-ray diffraction (XRD) was performed on a Bruker D8 DISCOVER diffractometer with Cu Kα radiation. Raman spectroscopy was carried out using a Renishaw 1000B Raman microscope with a 632.8-nm HeNe laser with three accumulations of 10 s each. The surface area measurements were carried out by Brunauer, Emmett, and Teller

(BET) $N_2$ adsorption/desorption on a Micromeritics ASAP 2020. The pore size was analyzed based on a quenched solid density functional theory (QSDFT) kernel applied to the adsorption branch using a slit-pore model. Fourier transform infrared (FTIR) spectroscopy was measured on a Nicolet 5700 FT-IR spectrometer in the range of wave numbers 400–4000 $cm^{-1}$ at a resolution 4 $cm^{-1}$. X-ray photoelectron spectroscopy (XPS) spectra of samples were obtained using a PerkinElmer PHI 5440 ESCA spectrometer with monochromatic Mg Kα radiation as the X-ray source.

To prepare the electrodes, the AC or the MPS-GO/AC was mixed with carbon black and polyvinylidene fluoride (PVDF) binder (72:8:20, by weight) in N-methyl-2-pyrrolidone (NMP) to form a homogeneous slurry. The resulting slurry was coated onto a graphite foil using a doctor blade method, dried under vacuum at 80 °C overnight, and cut to 4.2×4.2 square inches to obtain single-side electrodes. The mass loading of activated carbon on the single-side electrode was approximately 2.2 mg $cm^{-2}$. To prepare double-side electrodes, the carbon slurry was coated on the backside of the single-side electrode before cutting.

A single-pass model was used throughout this study. A CDI cell demonstrated in our previous report [1] was used to test the CDI performance of the MPS-GO/AC composite. The cell allows a radial flux through the CDI cell from bottom center to four corners of the anodes and finally out of the cell from top center. Feeding water was pumped to the CDI cell from a reservoir by a peristaltic pump at a flow rate of 23 mL $min^{-1}$, which was a measured value when the flow rate was set to be 25 mL $min^{-1}$ by the pump. Typically, a two-layer-electrode cell was composed of a double-sided anode sandwiched by two single-sided cathodes. In the cases of cells with more electrode layers, double-sided cathodes were added, together with more double-sided anodes. For example, an 8-layer-electrode cell was assembled with two layers of single-sided cathodes, three layers of double-sided cathodes, and four layers of double-sided anodes. The anodes consisted of MPG-GO/AC composite, while the cathode was composed of the AC. Only anion-exchange membranes (AEM) were applied to improve the removal efficiency and discharge efficiency. Silicone gaskets were used on each electrode layer to seal CDI cells. Cation exchange membranes (CEMs) were not used because lead ions can be trapped in the CEMs.[1] A voltage of -1.2 V and 1.2 V was applied to the CDI cell during charging and discharge processes, respectively, controlled by a CHI 670E electrochemical workstation. Note that to remove cations, the charge voltages for the working electrodes were set to be negative by the electrochemical potentiostat.

The ion concentration of the effluent water was measured by inductively-coupled plasma-optical emission spectroscopy (ICP-OES) according to the US EPA standard[2]. The removal efficiency and removal rate of each cation were calculated according to Equations S1 and S2, respectively:

$$e = \frac{c_0 - c}{c_0} \times 100\% \#(S1)$$

$$E\% = \frac{\int_0^t e dt}{t} \#(S2)$$

where $c$ represents the concentration at the given sampling time, $c_0$ is the initial concentration, and $t$ is the charging duration.

The discharge rate was calculated by comparing the discharged cations with the corresponding accumulated adsorbed cations:

$$De\% = \frac{(c_i - c_0)v}{ec_0t} \times 100\%\#(S3)$$

where $v$ is the volume of discharge effluent, and $c_i$ is the concentration of discharged cation.

Selective removal of $Pb^{2+}$ was indicated by the relative removal coefficient calculated based on Equation S4,

$$S = \frac{e_{Pb}}{e_B} \times \frac{c_B}{c_{Pb}} \quad (S4)$$

where $e_{Pb}$ and $e_B$ indicate the removal efficiency of $Pb^{2+}$ and the other species (e.g., $Ca^{2+}$ and $Mg^{2+}$), and $c_{Pb}$ and $c_B$ are their concentrations, respectively.

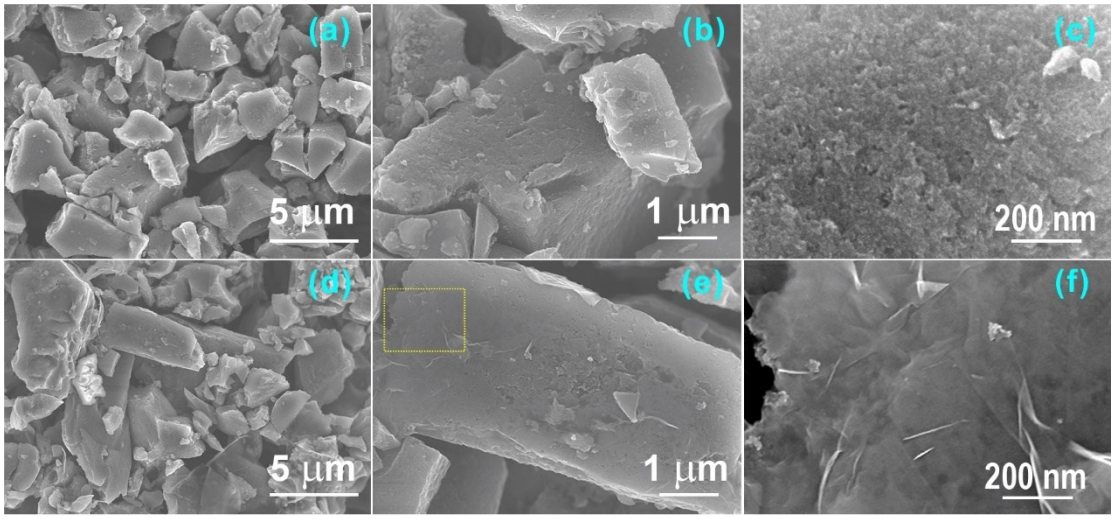


Figure S1. SEM images of (a-c) AC and (d-f) MPG-GO/AC. (f) was magnified from the yellow rectangle zone in (e), showing the surface of AC was coated by MPG-GO.

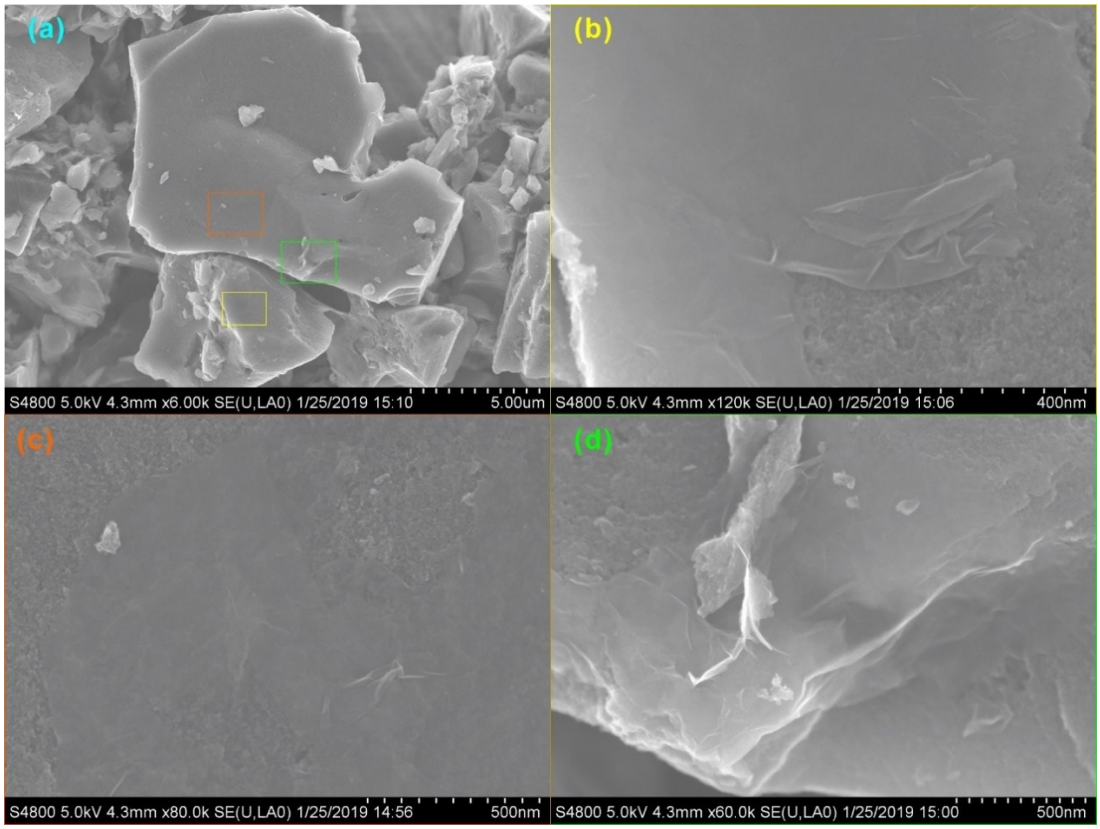


Figure S2. SEM images of MPG-GO/AC: (b), (c), and (d) were locally zoomed-out images, marked by yellow, orange, and green rectangles in (a).

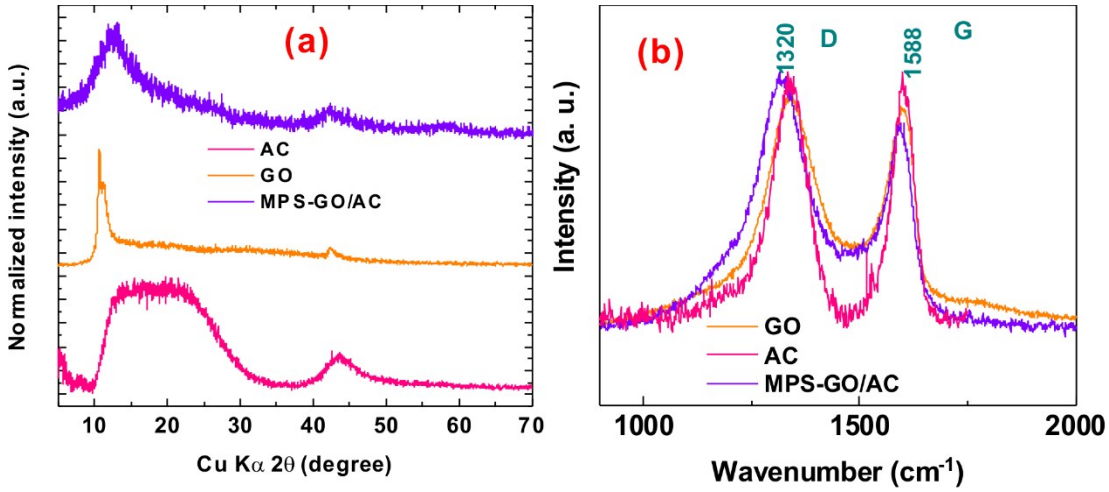


Figure S3. (a) XRD patterns and (b) Raman spectra of AC, GO, and MPS-GO/AC.

The AC and the MPG-GO/AC were examined by X-ray diffraction (XRD) and Raman spectroscopy. The AC shows a very broad peak at 10-30 ° in the XRD pattern (Figure S3a), which was indexed to 002 facet of graphitic carbon and was affected by the micropores in the AC [3]. The GO exhibits a sharp peak at 11 °, which is consistent with the literature [4]. By combining the effects of the AC and GO, the MPS-GO/AC composite showed the major peak at 12.6 °. Raman spectra of both the AC and the GO present D-band and G-band at 1,320 and 1,588 $cm^{-1}$, respectively (Figure S3b); however, compared with the AC, GO showed a much larger amount of defect carbon. As a result, the MPS-GO/AC composite exhibited a higher $I_D/I_G$ ratio than the AC (1.3 vs. 1.0).

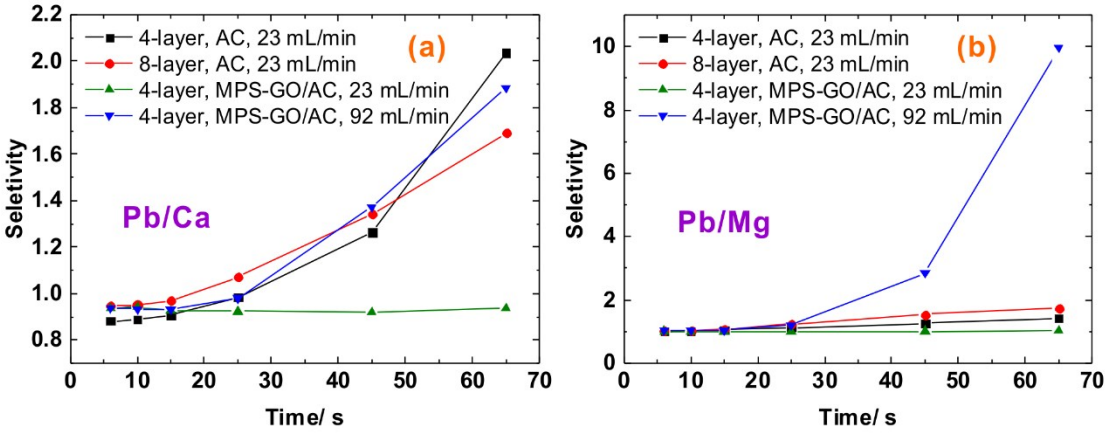


Figure S4. Removal selectivity of Pb against Ca (a) and Mg (b) using AC and MPS-GO/AC electrodes. Note that the CDI cells were subjected to 5-min wetting before starting charging. The timeline in the figures was consistent with that of Figure 2. As can be seen, selective removal of $Pb^{2+}$ against $Ca^{2+}$ and $Mg^{2+}$ was observed since ~20 min. As a matter of fact, the selectivity values were even smaller than 1, e.g., as shown in Figure S3a, which is due to the greater mobility of $Ca^{2+}$ than $Pb^{2+}$. The selective removal of $Pb^{2+}$ against $Ca^{2+}$ and $Mg^{2+}$ occurred at later charging stage because of the replacement mechanism of selective removal of $Pb^{2+}$ against $Ca^{2+}$ and $Mg^{2+}$, as we discussed in our previous report.[1] $Ca^{2+}$ and $Mg^{2+}$ can be electrosorbed on the electrode more quickly than $Pb^{2+}$ at early stage; but they will be replaced by $Pb^{2+}$ because of the stronger affinity of $Pb^{2+}$ with functional groups (such as carboxyl and thiol) than $Ca^{2+}$ and $Mg^{2+}$.

Table S1. Water quality of major cities (counties) in 2017

| | Lead (Pb) | | | Calcium (Ca) | | | Orthophosphate ($PO_4^{3-}$) | | |
|---|---|---|---|---|---|---|---|---|---|
| CITY (COUNTY) | Max* (μg/L) | Min. (μg/L) | Ave. (μg/L) | Max. (mg/L) | Min. (mg/L) | Ave. (mg/L) | Max. (mg/L) | Min. (mg/L) | Ave. (mg/L) |
| Milwaukee | 130 | 4 | 0.00 | 36.00 | 35.00 | 35.50 | 2.97 | 0.77 | 1.87 |
| Madison (Dane) | 118 | 0 | 2.29 | 110.00 | 45.30 | 67.15 | 0.29 | 0.15 | 0.22 |
| Kenosha | 95.7 | 0 | 2.49 | 85.00 | 0.57 | 32.99 | 0.09 | 0.08 | 0.08 |
| Green Bay (Brown) | 66 | 0 | 3.95 | 91.00 | 12.00 | 42.21 | 0.26 | 0.16 | 0.22 |
| Racine | 147 | 0 | 4.14 | 97.20 | 0.38 | 37.59 | 1.00 | 0.17 | 0.75 |
| Appleton (Outagamie) | 71 | 0 | 1.99 | 270.00 | 6.68 | 50.29 | 0.26 | 0.19 | 0.24 |
| Waukesha | 140 | 0 | 2.58 | 130.00 | 11.10 | 82.19 | 0.52 | 0.11 | 0.36 |
| Eau Claire | 39 | 0 | 1.97 | 62.10 | 0.05 | 15.56 | N/A | N/A | N/A |
| Oshkosh | 25 | 0 | 3.91 | 120.00 | 0.08 | 34.16 | 0.64 | 0.54 | 0.58 |
| Janesville | 470 | 0 | 4.63 | 93.00 | 0.29 | 64.49 | N/A | N/A | N/A |
| Chicago | <1 | <1 | <1 | 36.40 | 35.90 | 36.09 | 1.39 | <0.06 | 1.12 |
| New York | 3 | 0 | 0.00 | 30.20 | 5.10 | 7.30 | 3.00 | 0.70 | 2.10 |

Data of 10 Wisconsin counties were taken from dnr.wi.

*Maximum lead in Wisconsin were from first-draw samples at taps in 50 homes with lead services.

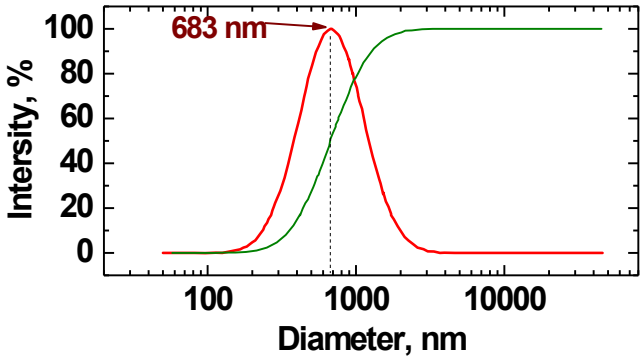


Figure S5. Mean particle size in tap water after addition of 1 ppm $Pb^{2+}$.

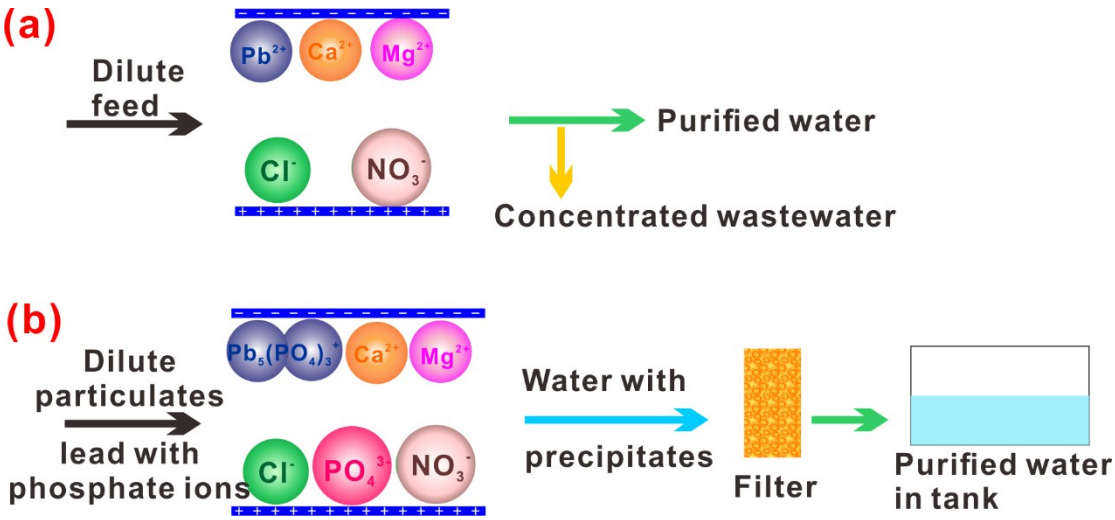


Figure S6. Illustration of typical CDI performance of (a) synthetic water without phosphate ions, and (b) tap water with phosphate additives.

Because of the very low solubility product constant of $Pb_3(PO_4)_2$ ($8.0\times10^{-43}$), the lead in tap water exists in the form of particulates after addition of phosphates, which leads to easier removal of lead during charging. More interestingly, upon discharging, the accumulated phosphate ions are released from the anode, together with the lead particulates discharged from the cathode, which results in formation of precipitates (Figure S6b). The precipitates can be removed by a filter.

Table S2. Literature comparison on removal of lead ions by CDI

| Materials | Mode | Water type | Investigated cations | $PO_4^{3-}$ related | Wastewater generation | Ref. |
|---|---|---|---|---|---|---|
| Activated carbon cloth | Batch | DI | $Cd^{2+}$, $Pb^{2+}$, and $Cr^{3+}$ | No | Yes | [5] |
| Fe3O4/porous graphene | Batch | crystal violet dye solution | $Pb^{2+}$, $Cu^{2+}$, and $Cd^{2+}$ | No | Yes | [6] |
| O-Doped boron nitride nanosheets | Batch | DI | $Zn^{2+}$, $Cd^{2+}$, $Pb^{2+}$, $Ni^{2+}$, $Co^{2+}$, $Cu^{2+}$, $Mg^{2+}$, $Ca^{2+}$, $Fe^{2+}$, $Fe^{3+}$ and $Na^{+}$ | No | Yes | [7] |
| EDTA or APTES-grafted graphene | Batch | DI | $Pb^{2+}$ and $Na^{+}$ | No | Yes | [8] |
| porous N-doped graphene | Batch | DI | $Pb^{2+}$, $Cd^{2+}$, $Cu^{2+}$, $Ni^{2+}$, $Zn^{2+}$, $Co^{2+}$, $Fe^{2+}$, $Mg^{2+}$, and $Ca^{2+}$ | No | Yes | [9] |
| Activated carbon (AC) | Single-pass | DI | $Pb^{2+}$, $Mg^{2+}$, and $Ca^{2+}$ | No | Yes | [1] |
| AC/MPS-GO | Single-pass | Tap water | $Pb^{2+}$, $Mg^{2+}$, and $Ca^{2+}$ | Yes | No | This work |

Note: DI represents de-ionized water

References:


[1] Q. Dong, X. Guo, X. Huang, L. Liu, R. Tallon, B. Taylor, J. Chen, Selective removal of lead ions through capacitive deionization: Role of ion-exchange membrane, Chem. Eng. J. 361 (2019) 1535-1542. https://dio.org/10.1016/j.cej.2018.10.208.

[2] US EPA Method 6010D – Inductively Coupled Plasma-Optical Emission Spectrometry, 2014, pp. 1-35.

[3] X.K. Huang, D. Liu, X.R. Guo, X.Y. Sui, D.Y. Qu, J.H. Chen, Phosphorus/Carbon Composite Anode for Potassium-Ion Batteries: Insights into High Initial Coulombic Efficiency and Superior Cyclic Performance, Acs Sustain Chem Eng 6 (2018) 16308-16314. https://dio.org/10.1021/acssuschemeng.8b03241.

[4] H. Yang, J. Jiang, W. Zhou, L. Lai, L. Xi, Y.M. Lam, Z. Shen, B. Khezri, T. Yu, Influences of graphene oxide support on the electrochemical performances of graphene oxide-$MnO_2$ nanocomposites, Nanoscale Res. Lett. 6 (2011) 531. https://dio.org/10.1186/1556-276X-6-531.

[5] Z. Huang, L. Lu, Z.X. Cai, Z.J. Ren, Individual and competitive removal of heavy metals using capacitive deionization, J. Hazard. Mater. 302 (2016) 323-331. https://dio.org/10.1016/j.jhazmat.2015.09.064.

[6] G. Bharath, E. Alhseinat, N. Ponpandian, M.A. Khan, M.R. Siddiqui, F. Ahmed, E.H. Alsharaeh, Development of adsorption and electrosorption techniques for removal of organic and inorganic pollutants from wastewater using novel magnetite/porous graphene-based nanocomposites, Sep. Purif. Technol. 188 (2017) 206-218. https://dio.org/10.1016/j.seppur.2017.07.024.

[7] M.M. Chen, D. Wei, W. Chu, T. Wang, D.G. Tong, One-pot synthesis of O-doped BN nanosheets as a capacitive deionization electrode for efficient removal of heavy metal ions from water, J. Mater. Chem. A 5 (2017) 17029-17039. https://dio.org/10.1039/c7ta05459a.
[8] P.Y. Liu, T.T. Yan, J.P. Zhang, L.Y. Shi, D.S. Zhang, Separation and recovery of heavy metal ions and salt ions from wastewater by 3D graphene-based asymmetric electrodes via capacitive deionization, J. Mater. Chem. A 5 (2017) 14748-14757. https://dio.org/10.1039/c7ta03515b.
[9] L.J. Liu, X.R. Guo, R. Tallon, X.K. Huang, J.H. Chen, Highly porous N-doped graphene nanosheets for rapid removal of heavy metals from water by capacitive deionization, Chem. Commun. 53 (2017) 881-884. https://dio.org/10.1039/c6cc08515f.